AGU PUBLICATIONS

JGR

Journal of Geophysical Research: Biogeosciences

RESEARCH ARTICLE

10.1002/2017JG003906

Key Points:
- Streams sampled on the eastern slopes of Wyoming's Bighorn range exhibited variable source/sink behavior
- Dissolved gas concentrations, especially methane, were higher in the Great Plains agricultural sites than in the forested Middle Rockies
- Spring snowmelt runoff and periods had significantly higher fluxes of carbon dioxide and methane than periods of base flow

Supporting Information:
- Supporting Information S1

Correspondence to:
C. Kuhn,
ckuhn@uw.edu

Citation:
Kuhn, C., C. Bettigole, H. B. Glick, L. Seegmiller, C. D. Oliver, and P. Raymond (2017), Patterns in stream greenhouse gas dynamics from mountains to plains in northcentral Wyoming, *J. Geophys. Res. Biogeosci.*, *122*, doi:10.1002/2017JG003906.

Received 18 APR 2017
Accepted 26 JUL 2017
Accepted article online 31 JUL 2017

©2017. American Geophysical Union. All Rights Reserved.

Patterns in stream greenhouse gas dynamics from mountains to plains in northcentral Wyoming

C. Kuhn[1,2], C. Bettigole[2], H. B. Glick[2], L. Seegmiller[2], C. D. Oliver[2], and P. Raymond[2]

[1]School of Environmental and Forest Sciences, University of Washington, Seattle, Washington, USA, [2]School of Forestry and Environmental Studies, Yale University, New Haven, Connecticut, USA

Abstract Quantification of small stream contributions to global carbon cycling is key to understanding how freshwater systems transmit and transform carbon between terrestrial and atmospheric pools. To date, greenhouse gas emissions of carbon dioxide and methane from freshwaters, particularly in mountainous regions, remain poorly characterized due to a lack of direct field observations. Using a unique longitudinal approach, we conducted field surveys across two ecoregions (Middle Rockies and Great Plains) in the Clear Creek watershed, a subwatershed of Wyoming's Powder River Basin. We took direct measurements of stream gases using headspace sampling at 30 sites (8 June to 23 October). We observed the lowest and most variable concentrations in headwaters, which flow through a federally designated alpine wilderness area. By contrast, the Great Plains exhibited 1.45 and 4 times higher pCO_2 and pCH_4 concentrations and the relative contributions of methane increased downstream. Fluxes during snowmelt were 45% and 58% higher for CO_2 and CH_4 than during base flow but overall were lower than estimates for other systems. Variability for pCO_2 was highest during late summer and in the uppermost sections of the headwaters. The high heterogeneity and common undersaturation observed through space and time, especially in the mountains, suggest that downscaled regional estimates may fail to capture variability in fluxes observed at these smaller scales. Based on these results, we strongly recommend higher resolution time series studies and increased scrutiny of systems at near equilibrium, inclusive of winter storage and ice-off events, to improve our understanding of the effects of seasonal dynamics on these processes.

Plain Language Summary This study documents trends in methane and carbon dioxide dynamics in a small stream in Wyoming based on field-collected samples gathered over the length of the stream. This research is important because streams have been shown to emit significant amounts of greenhouse gases. Our results show, however, that this stream can both emit and take up carbon gasses and that this behavior varies through time and space.

1. Introduction

In the last two decades, rivers, lakes, and streams have become firmly established as active transformation sites for land carbon that are often net sources of atmospheric carbon gases [*Cole et al.*, 2007; *Bastviken et al.*, 2011]. Inland waters globally outgas a total of 1.4–2.1 Pg CO_2 and 0.65 Pg of CH_4 as CO_2 equivalents annually [*Raymond et al.*, 2013; *Aufdenkampe et al.*, 2011; *Bastviken et al.*, 2011; *Cole et al.*, 2007], an amount greater than downstream transport [*Houghton et al.*, 2012; *Wallin et al.*, 2010; *Algesten et al.*, 2004]. New research by *Sawakuchi et al.* [2017] indicates that global inland water CO_2 emissions may be up to 43% higher than previously thought due to newly documented contributions from the Amazon Lower Basin. Despite the significant role inland waters play in global carbon budgets, methodological questions related to the estimation of gas transfer velocities, the characterization of surface water extent, and differences in measurement protocols contribute to large uncertainties in estimations of carbon fluxes along the land to ocean continuum [*Butman et al.*, 2016]. Research efforts have quantified spatiotemporal drivers of dissolved CO_2, contributions of CO_2 to total carbon export in boreal systems [*Wallin et al.*, 2013; *Wallin et al.*, 2011; *Striegl et al.*, 2012; *Campeau and Del Giorgio*, 2014], and carbon loss through outgassing in tropical systems [*Borges et al.*, 2015; *Richey et al.*, 2002; *Mayorga et al.*, 2005; *Johnson et al.*, 2008]. However, CO_2 and CH_4 dynamics in mountainous and agricultural regions remain understudied [*Bodmer et al.*, 2016].

Small streams in particular act as exchange hot spots between aquatic and atmospheric stores. Lower order streams collectively contribute 20–50% of the total stream network surface area available for gas exchange [*Butman and Raymond*, 2011; *Bishop et al.*, 2008] and have been recently estimated to contribute 36% of

total outgassing from rivers and streams [*Marx et al*., 2017]. Lower order streams exhibit high hydrologic connectivity and biogeochemical reactivity, bridge the soil/water interface, and process land carbon for burial, advection, or emissions [*Wallin et al*., 2010; *Jones and Mulholland*, 1998; *Genereux and Hemond*, 1992]. The exchange can occur on small spatial scales; in some systems between 65 and 90% of groundwater heavily laden with dissolved inorganic carbon (DIC) can outgas within a few hundred meters of the soil/stream interface [*Johnson et al*., 2008; *Öquist et al*., 2009]. However, small stream pCO_2 and pCH_4 values, especially in mountains and agricultural lands, are underreported [*Crawford et al*., 2015; *Schade et al*., 2016; *Marx et al*., 2017] and poorly constrained, with published estimates varying widely [*Finlay*, 2003; *Butman and Raymond*, 2011; *Stackpoole et al*., 2014; *Hope et al*., 2004].

Current research efforts reporting longitudinal trends in gas concentrations across different systems often reach different conclusions [*Striegl et al*., 2012; *Campeau andand Del Giorgio*, 2014] as to whether fluxes and concentration increase or decrease along a downstream gradient, pointing to a need for more studies to resolve patterns and drivers across a spectrum of geomorphic, ecological, and land use types. Dramatic seasonal shifts in flow regime driven by spring snowmelt pulses further complicate these controls by adding a hydrologic dimension [*Ågren et al*., 2010], indicating the importance of integrating hydrology as a master control for in-stream carbon dynamics [*Dawson et al*., 2008]. Landscape scale studies can therefore provide a broader view of the space-time controls on these complex riverine relationships that govern carbon pools [*Tamooh et al*., 2014; *Richey*, 2004; *Allan*, 2004].

The Bighorn Mountains provides a natural laboratory for studying changes in stream chemistry across a wide variety of landscapes. On the eastern slopes of the mountains, headwater streams traverse downslope along an ecological, geomorphic, and land use gradient. Originating in pristine, federally protected alpine wilderness restricted to nonmotorized vehicle use, streams leaves the mountains to enter residential communities and agricultural rangelands. These headwater networks transport and transform snowmelt and terrestrial materials for downstream users. Studies in other regions have shown that as catchment area and discharge increase, controls such as in situ microbial respiration, the decay of terrestrial organic material, and dissolution of carbonates may vary [*Humborg et al*., 2010; *Palmer et al*., 2001; *Dinsmore and Billett*, 2008]. Concurrently, human activities including urbanization, crop production, grazing, natural gas development, and timber harvesting increase with decreasing elevation. Industrialization, urbanization, and agricultural activities can mobilize aged carbon stocks and are thought to increase carbon flux in aquatic systems globally by an added 0.1–0.2 Pg carbon per year [*Butman et al*., 2014]. Streams in human-disturbed landscapes display elevated CO_2 levels [*D'Amario and Xenopoulos*, 2015], rising stream temperatures [*Kaushal et al*., 2010], increased silica fluxes [*Carey and Fulweiler*, 2012], and higher dissolved inorganic carbon export [*Barnes and Raymond*, 2009]. This highlights a need to document, at higher spatial and temporal resolutions, current biogeochemical dynamics as aquatic systems increasingly experience human disturbance and other global change pressures, especially as a warming climate brings changes to annual stream discharge and runoff timing [*Cayan et al*., 2016; *Mote et al*., 2005].

In this work, we present a study addressing trends in dissolved greenhouse gas concentrations and fluxes in a headwater stream network as it increases in size and traverses across a wilderness to agricultural landscape continuum. Findings from this large data set feature both pCO_2 and pCH_4 (n = 702) measurements and include samples taken at some of the highest elevations (3311 m) reported in the literature. Our study in northcentral Wyoming seeks to (1) quantify the distribution of surface water greenhouse gas concentrations (pCO_2 and pCH_4) in order to provide initial measurements in an understudied region; (2) test how basin characteristics, discharge, and elevation shape the observed CH_4 and CO_2 dynamics and emissions in this fluvial network; and (3) estimate gas transfer velocities and CH_4 and CO_2 diffusive fluxes. By undertaking this field study and analysis, we aim to provide new field measurements to inform regional scaling and to provide insight into the spatial and temporal dynamics of dissolved carbon gases for this system.

2. Materials and Methods

2.1. Site Description

Clear Creek (Figure 1) originates in a small alpine lake (3311 m) in the Bighorn Mountains and flows east-northeast into the semiarid Great Plains (1211 m), reaching its confluence with the Powder River north of Arvada, WY. Similar to other drainages on the eastern flank of the range, the stream straddles two

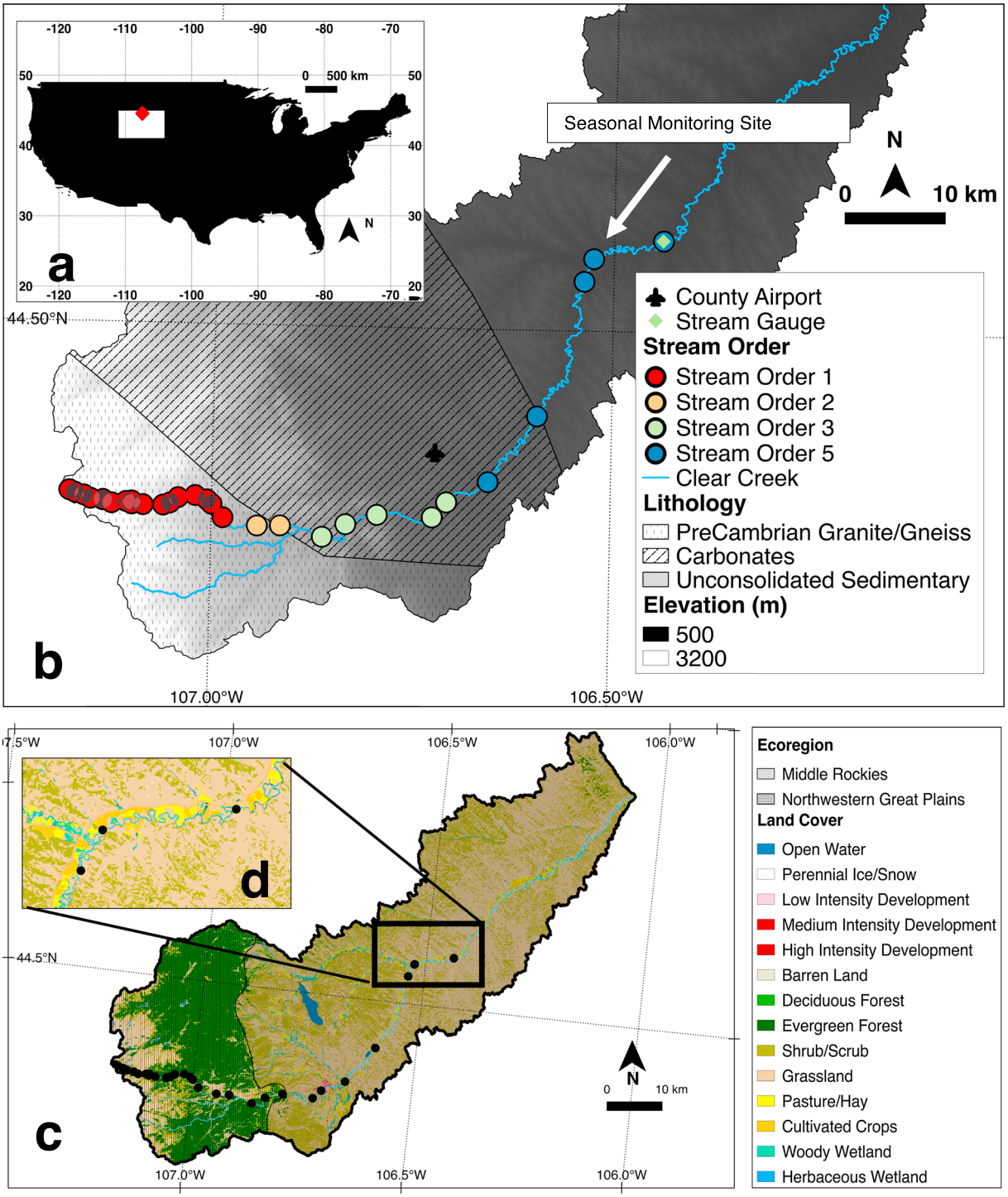

Figure 1. Study site. (a) Site location within the state of Wyoming in the United States. (b) The central study watershed showing underlying lithology, stream order, and elevation for each sampling site. (c) Land use and ecoregion designation with subset (d) showing the cultivated and grazed riparian areas found in the Plains. Five subsites located at the Big Red site (Site 2) on the Ucross Ranch were used for sampling at higher temporal frequencies as indicated by the label and arrow in Figure 1b.

ecoregions—the alpine Middle Rockies upland and the Northwestern Great Plains lowlands. The subalpine forested uplands feature bands of Engelman spruce (*Picea engelmanii*) and subalpine fir (*Abies lasiocarpa*), with lodgepole (*Pinus contorta*) and ponderosa pine (*Pinus ponderosa*) at lower elevations [*Weaver*, 1980;

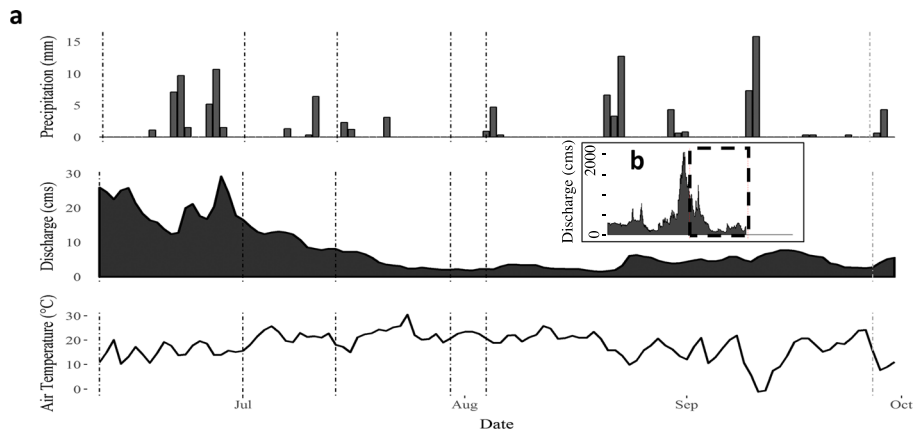

Figure 2. (a) Climatic and hydrologic trends during the 1 June to 1 October sampling season. Precipitation and temperature data were obtained from observations made at the Johnson County Airport (KYBG) in Buffalo, WY, and quality controlled by NOAA's National Climactic Data Center. The vertical dashed lines in Figure 2a (top) indicate primary sampling dates. (b) The 2014 annual hydrograph shows our sampling period, indicated by dashed lines in Figure 2b which took place during the decline of peak snowmelt and into the period of late summer base flow. The period of record for this gauge ends on 3 October, which is the end of the water year for the Wyoming State Engineer's Office.

Logan and Irwin, 1985]. Catchment lowlands are dotted with shrubs, forbs, and Wyoming big sagebrush (*Artemisia tridentate wyomingensis*) habitat [*Doherty et al*., 2008; *Taylor et al*., 2012]. Clear Creek originates above treeline in granitic gneiss, descends through Bighorn dolomite and Madison limestone before entering the alluvial carbonate floodplain [*Survey*, 2014]. Land use in the Plains (Table S1 in the supporting information) is predominantly devoted to ranching, livestock production, and irrigated agriculture [*BLM*, 2002; *Stearns et al*., 2005], while the Rockies are mostly forested (Table S1). Temperatures range (Figure 2) from to −39°C to 40°C [*Mapel*, 1959] with an annual average of 7.4°C [*Climate*, 2016]. Annual precipitation ranges from 37 cm to 76 cm with more precipitation, mostly as snow, at higher elevations [*Swenson*, 1953]. Spring snowmelt runoff from the mountains dominates streamflow, with occasional contributions from summer storms. During the spring and early summer, ephemeral creeks form in the lowland draws. At 50.6 river kilometers (Figure 1), the stream passes through Buffalo, WY (pop 4585) where flows are doubled by Rock Creek and by efflux from the City Water Treatment plant.

2.2. Sampling Design

This study focuses on the main stem of one headwater stream (Clear Creek) and its tributaries (Figure 1). Our study design includes two data sets, one designed to capture spatial variability and the second collected at a higher temporal resolution at just one site. For the first spatial data set (indicated by $n = 449$), we established 30 sampling sites (Figure 1) along an altitudinal and wilderness-to-agricultural land use gradient from the headwaters (3311 m above sea level (asl)) to the Plains (1211 m asl) at approximately every 40 m change in elevation. We sampled from the bank at all 30 fixed sites (Tables 1 and 2) along this transect on six separate events beginning during the descending limb of spring flooding (8 June 2014) and ending in the fall (23 October 2014) (Figure 2). Discussions of spatial variability will focus on this longitudinal data set identifiable by sample size of 449 when not referred to as the longitudinal data set.

To capture seasonal changes with higher temporal frequency, we monitored a subset of five sites approximately 15 m apart within Site 2 (Big Red) approximately twice weekly (25 times) from late spring to early fall (11 June 2014 to 23 October 2014). We chose Site 2 (Figure 1b) because of its ease of access and proximity to the U.S. Geological Survey (USGS) gauging station. Discussions of seasonal trends will focus on this subset of five sites, henceforth referred to as the seasonal data set (and indicated by an n of 253) where we have higher temporal resolution sampling data. In order to reduce noise from diel signatures, sampling was conducted during morning hours. Atmospheric samples were collected throughout the field season to establish ambient gas concentrations for solubility calculations ($n = 13$). The longitudinal data set ($n = 449$) was used to analyze spatial variability at course time scales, and the higher temporal resolution seasonal data set ($n = 253$) was used to analyze seasonal changes.

Table 1. This Table Describes Key Subbasin Characteristics[a]

Site	Name	Distance From Headwater (km)	Elevation (m)	Area[b] (km^2)	Stream Order	Agriculture[c] (%)
1	Double Cross (P)	191	1211	1789	5	17.08
2	Big Red (P)	168	1235	1715	5	12.78
3	Vignaroli (P)	160	1245	1056	5	10.24
4	Gordon (P)	115	1314	927	5	6.43
5	Rock Creek (P)	92	1366	849	5	4.29
6	City Park (P)	81	1416	347	3	0.64
7	Chokecherry Lane (P)	77	1453	317	3	1.10
8	McNeese Access (R)	66	1632	309	3	0.00
9	Mosier Gulch (R)	60	1747	293	3	0.00
10	Grouse Mountain (R)	52	1976	264	3	0.00
11	Chris Kanodle (R)	43	2127	80	2	0.00
12	Hunter Trailhead (R)	39	2206	76	2	0.00
13	Buffalo Park (R)	32	2398	42	1	0.00
14	Four Lakes (R)	29	2573	39	1	0.00
15	Soldier Graves (R)	28	2616	39	1	0.00
16	Soldier Park (R)	25	2642	37	1	0.00
17	Wilderness Boundary (R)	22	2716	35	1	0.00
18	Moose Meadow (R)	20	2760	33	1	0.00
19	Seven Brothers (R)	19	2781	32	1	0.00
20	Bear Bend (R)	15	2818	27	1	0.00
21	Thousandth Bite[b] (R)	13	2842	26	1	0.00
22	Deer Lake (R)	12	2844	21	1	0.00
23	Brook Trout (R)	11	2870	19	1	0.00
24	Boulder Field (R)	8	2900	17	1	0.00
25	Powell Junction (R)	6	2929	15	1	0.00
26	Powell Creek* (R)	6	2929	12	1	0.00
27	Medicine Park (R)	4	3035	7	1	0.00
28	Abracadabra (R)	3	3133	6	1	0.00
29	Vanishing Creek (R)	1	3261	4	1	0.00
30	Florence Lake (R)	0.00	3311	4	1	0.00

[a]Sites are listed in order of increasing elevation and proximity to the headwaters. Percentages are reported for each site's cumulative subbasin area inclusive of upstream basin statistics. Sites classified as tributaries to the main fork are indicated by an asterisk. Ecoregion is indicated by either a (P) Great Plains or (R) Middle Rockies listed next to site name. Sites within the nonmotorized vehicle wilderness boundary include all sites past the wilderness boundary.
[b]Total drainage area, computed by summing subbasin area and all the upstream catchments.
[c]Includes both cultivated crops and pasture/hay as a percent of the individual catchment area.

2.3. Hydrology and Basin Delineations

Flow data for the study period was collected from four former USGS gauging stations (118.83, 111.28, 115.07, and 51.38 river kilometers), now operated by the Wyoming State Engineer's Office. We delineated the watershed boundary using the ArcHydro data model embedded in the ArcGIS platform [*Environmental Systems Research Institute Inc*, 2008] and a USGS 8.9 m resolution digital elevation model [*Gesch et al*., 2002]. Each sampling point was snapped to the National Hydrography Dataset Plus (NHDPlus) stream network [*Simley and Carswell*, 2009] and assigned a catchment polygon encompassing its entire upstream drainage area. Stream order was extracted from the NHDPlus. Due to terrain steepness and private property restrictions, no fourth-order stream segments were sampled. These polygons were used as inputs into a zonal statistics functions to determine total drainage area, mean catchment slope, reach-averaged slope, and percent coverage of each land use type (Table S1) from the 2006 National Land Cover Dataset [*Xian et al*., 2011]. Total upstream wetland cover at each drainage point was calculated from the U.S. Fish and Wildlife's 2014 National Wetlands Inventory data set [*Service*, 2009]. Underlying carbonate composition (Table S1) was determined using zonal statistics and a global surficial lithology data set [*Dürr et al*., 2005], in which a region is classified as carbonate if it is composed of sedimentary rock with higher than 50% carbonate concentration. Watershed development is an National Land Cover Dataset land cover classification derived from satellite remote sensing that indicates areas of human settlement and urbanization [*Fry et al*., 2011].

Table 2. Observed Stream Properties and Computed Hydraulic Geometries Averaged Over the Sampling Season From 11 June to 23 October 2014 for Each Site in the Longitudinal Data Set (n = 449)[a]

Site	% TWA [b]	Stream Temp (°C)	pH	Slope[c]	Width (m)	Depth (m)	Specific Discharge (cm km^{-2})	pCH_4 (uatm) (SD)	pCO_2 (uatm) (SD)
1	4.17	15.61	8.12	2.20	10.62	0.27	0.42	5.2 (3.9)	761 (157)
2	36.82	14.18	8.10	2.48	15.59	0.63	0.47	3.4 (2.2)	642 (107)
3	7.22	14.78	8.13	2.89	11.60	0.33	0.73	6.4 (4.9)	797 (191)
4	4.36	14.60	8.17	1.95	10.67	0.27	0.44	12.6 (6.3)	542 (101)
5	28.06	13.43	8.17	2.43	14.41	0.53	2.83	1.6 (0.8)	467 (109)
6	1.57	13.13	7.94	2.86	9.08	0.19	0.16	3.8 (4.3)	427 (109)
7	0.57	12.88	7.86	5.24	7.73	0.13	0.06	0.9 (0.5)	350 (87)
8	0.9	11.40	7.69	7.50	8.29	0.16	0.09	0.7 (0.5)	372 (123)
9	1.61	11.48	7.76	12.46	9.22	0.20	0.17	1.1 (0.5)	301 (110)
10	10.26	11.30	7.72	7.44	11.65	0.33	0.70	0.9 (0.3)	302 (43)
11	0.25	9.65	7.67	5.52	6.74	0.10	0.02	0.8 (0.4)	323 (50)
12	1.90	9.88	7.59	7.69	9.35	0.2	0.19	0.8 (0.4)	558 (495)
13	0.15	8.08	7.66	8.12	6.24	0.08	0.01	0.7 (0.4)	748 (999)
14	0.01	7.41	7.75	5.51	4.05	0.03	0.00	0.7 (0.4)	371 (197)
15	0.09	7.15	7.52	1.94	5.71	0.07	0.01	6.1 (2.1)	397 (115)
16	0.12	6.62	7.61	3.75	6.10	0.08	0.01	0.7 (0.3)	432 (359)
17	0.12	7.08	7.42	4.51	6.04	0.08	0.01	0.6 (0.3)	282 (69)
18	0.07	7.55	7.43	2.81	5.35	0.06	0.01	1.2 (0.5)	299 (126)
19	0.26	7.36	7.71	2.35	6.70	0.10	0.02	1.5 (0.9)	268 (64)
20	0.09	7.33	7.07	4.17	5.70	0.07	0.01	0.8 (0.3)	302 (86)
21	0.25	8.01	7.01	4.17	6.09	0.08	0.01	2.7 (2.1)	800 (352)
22	0.09	7.10	7.75	4.21	5.70	0.07	0.01	0.7 (0.3)	314 (95)
23	0.15	7.77	8.02	2.52	5.61	0.07	0.01	0.7 (0.3)	754 (824)
24	0.10	7.30	7.53	5.79	5.28	0.06	0.00	0.6 (0.3)	272 (42)
25	0.18	6.83	7.41	8.79	5.74	0.07	0.01	0.6 (0.3)	287 (77)
26	0.29	7.62	8.04	6.83	6.38	0.09	0.01	0.5 (0.3)	274 (76)
27	0.05	7.10	7.87	13.14	4.65	0.04	0.00	0.5 (0.2)	186 (28)
28	0.07	6.23	6.63	16.31	4.94	0.05	0.00	0.5 (0.3)	308 (95
29	0.04	7.08	7.35	9.45	4.42	0.04	0.00	0.5 (0.3)	462 (480)
30	0.20	7.52	7.8	2.80	5.84	0.07	0.01	0.9 (0.7)	47181)

[a]Dissolved gas concentrations show the mean concentrations and standard deviation.
[b]% total watershed area.
[c]Reach-averaged slope.

2.4. Dissolved Gas Concentrations

Aquatic pCO_2 and pCH_4 concentrations (Table 2) were collected using a headspace equilibration method [*Hope et al.*, 1995; *Striegl et al.*, 2012; *Kling et al.*, 1991]. Triplicate samples of 40 mL bubble-free water were collected in 60 mL polypropylene syringes fitted with Luer lock three-way stopcocks and equilibrated with 20 mL of ambient air by shaking for 2 min at 0.1 m depth to maintain temperature. Fifteen milliliter of the resulting well-mixed headspace was then evacuated into a polypropylene 30 mL syringe fitted with a two-way Luer lock stopcock, and 15 mL was transferred into preevacuated 12 mL Exetainer glass vacuum vial (High Wycombe, UK). Exetainers were leak-tested and showed a leak rate of 0.5 and 1% per month for pCH_4 and pCO_2, respectively. We calculated ambient air gas concentrations by averaging atmospheric samples collected at the start and finish of each survey day. Air and water temperature, stream pH, conductivity, total dissolved solids, and salinity were simultaneously measured during each sampling event using an Oakton multiparameter handheld PC Tstr 35 probe and a digital thermometer equipped with a submersible probe.

We analyzed our samples using a Shimadzu GC-2014 Gas Chromatograph equipped with a flame ionization detector set to 100°C. The GC-2014 has an oven temperature set to 380°C and uses mephypulated helium (4.137e+6 Pa) as a carrier gas with a flow rate of 21 mL min^{-1}. Headspace concentrations were estimated through calibration against peak areas of standard samples with known concentrations. We used our in situ atmospheric observations (mean = 386 μatm for pCO_2 and 1.28 μatm for methane) to calculate the equilibrium aquatic concentrations used in the headspace calculation corrected for dilution. From the

headspace concentrations and ambient samples, dissolved aquatic gas concentrations (C_w; mg L^{-1}) were calculated using Henry's law:

$$[C_w] = p_{gas}{}^{*}\ kH \tag{1}$$

where the aqueous phase concentration of carbon dioxide or methane (C_w; mg L^{-1}) is a function of the partial pressure ($p_{gas;}$ μatm) of the respective gas and Henry's constant (kH) at a given temperature and salinity. kH is derived from field-collected air and water temperatures (Table 2) and barometric pressure observations, corrected for changes in elevation [*Manahan*, 1993], from the Buffalo, WY, airport weather station. This airport is located in the middle of our transect approximately 8.05 km from the Rock Creek site in the transition zone between the agricultural land use areas and the forested uplands of the higher elevation sites.

2.5. Calculating Flux

While carbon gas exchange can occur through diffusion and, in the case of methane, ebullition, plant-mediated transport, and possibly microbubbling [*McGinnis et al*., 2015; *Stanley et al*., 2015; *Prairie and del Giorgio*, 2013], our study focused on diffusive flux, empirically derived using a modified Fick's first law equation as follows:

$$\text{Flux} = (C_w - C_a)^{*}\ k_{gas} \tag{2}$$

in which diffusive flux (mol m^{-2} d^{-1}) is controlled by the concentration gradient at the water/air ($C_w - C_a$; mol m^{-3}) interface and the gas transfer velocity (k_{gas}; m s^{-1}) [*Raymond et al*., 2000]. We obtained a gas transfer velocity (k) normalized to a Schmidt number of 600 (k_{600}) using

$$k_{600} = VS \times 2841 \pm 107 + 2.02 \pm 0.209 \tag{3}$$

where V is stream velocity (m s^{-1}) and slope (S) expressed as a percent [*Raymond et al*., 2012] (r^2 = 0.55; Table 2). In order to determine velocity for equation (3), we used hydraulic geometry relationships representative of the Middle Rockies region based on the following power relationship developed by *David et al*. [2010]:

$$\text{Velocity} = 0.19^{*}\ Q^{0.49} \tag{4}$$

Direct measurements of flux with floating chambers or tracers were not feasible given the terrain and large spatial coverage of this sampling campaign. USGS discharge (Q; m^3 s^{-1}) was scaled to the drainage area for each sampling point data from USGS gauge (#06323550), now operated by the Wyoming State Engineer's Office (Figure 1). The final gas transfer velocity was calculated by normalizing the gas exchange velocity (m d^{-1}) for each gas (k_{gas}) to a Schmidt number at 600 (k_{600}) by correcting for temperature using Schmidt number dependencies (equation (5)) of CO_2 at 20°C in freshwater. The Schmidt number exponent (n) was assigned a value of 0.5, which represents the typical boundary layer conditions for this type of stream [*Wallin et al*., 2011]. We used the following equation originally developed by *Jähne et al*. [1987]:

$$k_{600} = k_{gas}\left(600/\text{Sc}_{gas}\right)^{-n} \tag{5}$$

The Schmidt number for CO_2 and CH_4 (Sc_{gas}) in equation (5) was calculated using field-observed temperatures and the equations from *Raymond et al*. [2012].

2.6. Statistical Techniques

Statistical analysis was conducted using the open-source RStudio version 0.99.903 [*R Development Core Team*, 2015]. Summary statistics were calculated using the "psych" packages [*Revelle*, 2016], and the gas transfer velocity models were fit using simple linear regression. We characterized uncertainty by reporting the mean, range, and standard deviation for estimated variables. To compare mean concentrations and fluxes between sites and sampling foray categories, we used repeated measures analysis of variance (ANOVA) with a Tukey's honest significant difference post-hoc test [*Tukey*, 1949] with a minimum significance level of 5% (α = 0.05) from the car package [*Fox and Weisberg*, 2011]. To assess the impact of bivariate catchment characteristics (e.g., ecoregion and presence of agriculture), Welch's two-sample t tests (WT) were used with a conservative minimum significance level of 5% (α = 0.05) and the assumption of nonequal variance. In plots where data were log transformed for visual clarity, untransformed versions are available in the supporting information.

3. Results

3.1. Site Context

Overall, sites exhibited a range of reach-averaged slopes (mean = 5%, range = 2–16%) with higher-elevation sites generally possessing higher slopes (Table 2). Stream temperatures during the sampling period averaged 10.17°C (2.5–21.2°C) (Table 2). Conductivity ranged from 0.00103 S/m at higher elevation sites to 0.0783 S/m at the lowland sites with an average of 0.0109 S/m (Table 2). Mean pH ranged from 7.6 in the headwater sites to 7.8 for the lower elevation sites (Table 2), suggesting that bicarbonate, not carbon dioxide, comprises the majority of the dissolved inorganic carbon (DIC) present in the stream, unlike more acidic organic-rich systems [*Kokic et al.*, 2015; *Abril et al.*, 2015; *Marx et al.*, 2017] that feature a lower pH with larger contributions of pCO_2 to the total DIC pool.

Mean daily flow at the watershed outlet (USGS #06323550, Site 1 in Figure 1) was 15.2 $m^3\ s^{-1}$. Flows peaked at 58.7 $m^3\ s^{-1}$ during spring snowmelt in early June (Figure 2). Minimum flows (1.3 $m^3\ s^{-1}$) occurred in late August during maximum agricultural withdrawals and high temperatures. We started our sampling 11 days after the highest observed spring discharge in early June (Figure 2) once it was safe to enter the floodplain. Between the uppermost gauge and the downstream outlet gauge, flows increase by 40% as several large tributaries join the stream. Flow data extend only until 1 October, as the State Engineer's Office ceased gauge operations at Double Crossing at that date. Year 2014 had higher discharge than the annual decadal average, especially in the months of May, June, and October. October discharge was more than twice as high as normal (48 $m^3\ s^{-1}$ versus 22 $m^3\ s^{-1}$ decadal mean). May, June, and July were 47–70% higher than the decadal mean.

3.2. Overall Aquatic Gas Concentrations

Throughout all data, we observed both supersaturation and undersaturation of both gases with respect to the atmosphere. The average pCO_2 equilibrium concentration was 538 μatm (μatm: range = 114–3223 μatm, $n = 702$). For pCH_4, mean values were 4.7 μatm (range = 0.13–70 μatm). These values represent 1.4 (pCO_2) and 3.7 (pCH_4) times above the atmospheric equilibrium concentrations (386 μatm for pCO_2 and 1.28 μatm for pCH_4) we observed in the field. pCO_2 and pCH_4 were supersaturated with respect to the atmosphere for 55% and 59% of all collected samples, respectively, including the longitudinal and seasonal data sets. The median was lower than the mean for both gases ($n = 702$). The means of pCO_2 and pCH_4 were significantly different (WT, $n = 702$, $t_{5,\ 95} = -96.93$, $P < 0.0001$), suggesting that the two gases do not share a distribution.

3.3. Gas Transfer Velocities and Fluxes

For the longitudinal study we sampled along a total stream network length of 191.22 km draining a watershed area of 1789 km^2 ($n = 449$). Mean stream width, as estimated using hydraulic geometry, increased by an order of magnitude from the first (mean: 1.5 m) to the fifth order (mean: 13.1 m) and averaged 4.85 m across the fluvial network (Table S2). This represents a total stream surface area of 1.92 km^2, which is <0.2% of the total area of the watershed at a drainage density of 0.12 km km^{-2}.

Using these geometries, we estimated the mean gas transfer velocity (k_{600}) across sites ($n = 449$) as 9.8 m d^{-1} (SD = 9.6 m d^{-1}) with higher mean values observed in the Great Plains ecoregion (Table 3). During our sampling, the stream network taken as an average acted as a net source (Table 3) of CO_2 and CH_4 but exhibited high spatiotemporal variability. CO_2 flux was on average 107 mmol $m^{-2}\ d^{-1}$ (−125 to 566 mmol $m^{-2}\ d^{-1}$), and 55% of samples were net sources of CO_2 ($n = 702$). CH_4 efflux and uptake were also both observed with a range and a mean of 2.43 mmol CH_4 $m^{-2}\ d^{-1}$ (−1.2 to 48 mmol $m^{-2}\ d^{-1}$), and 59% of all samples were sources of CH_4 ($n = 702$). Means for fluxes did significantly differ between the two gases (WT, $n = 702$, $t_{5,\ 95} = 33.855$, $P < 0.0001$). Spatially, this flux, especially for CH_4, was fueled largely by emissions from Great Plains sites (Table 3) and from emissions during snowmelt periods. We observed less consistent fluxes in the Middle Rockies, as many sites acted as net sinks for one or both gases (Figure 5).

3.4. Spatial Trends

In the longitudinal data set, log-transformed data showed differences in mean saturation between the Northwestern Great Plains and the Middle Rockies for both pCO_2 (WT, $n = 449$, $t_{5,\ 95} = 11.59$, $P < 0.0001$) and pCH_4 (WT, $n = 449$, $t_{5,\ 95} = 11.989$, $P < 0.0001$) (Table 3 and Figure 5). Northwestern Great Plains

Table 3. Ecoregion Summary Statistics[a]

	Northwestern Great Plains				Middle Rockies			
Name	Mean	Median	Range	SD	Mean	Median	Range	SD
pCO_2(μatm)	570	531	200–1095	202	391	293	114–3293	369
pCH_4(μatm)	4.90	1.98	0.24–26	2	1.19	0.92	0.12–9.9	5
FCO_2(mmol m^{-2} d^{-1})	79.46	59.51	−58–350	86	−1.77	−9.55	−125–566	67
			−0.36–7.58	2	−0.05	−0.004	−1.2–48	0.19
FCH_4(mmol m^{-2} d^{-1})	1.37	0.24						
k_{600}m d^{-1}	13.5		114.87–42.03	67.00	8.38	4.62	2.48–53.52	113

[a]Values reported for each ecoregion (n, Plains = 125, Rockies = 324) averaged over sites (30) and sampling runs (7) for the longitudinal data set (n = 449).

stream segments showed higher pCO_2 and pCH_4 concentrations than the Middle Rockies by 178 μatm pCO_2 (+145%) and 3.7 μatm (+410%) pCH_4. While all sites except one (Chokecherry Lane) in the Great Plains were supersaturated for both gases and also had positive fluxes, many sites in the Middle Rockies were undersaturated or only weakly saturated for either gas and exhibited uptake (Tables 3 and 2). The Middle Rockies sites exhibited higher standard deviation (Table 3) than the Great Plains sites for concentrations, fluxes, and gas transfer velocities. Lower variability in the Great Plains sites could be due to carbonate buffering. Only 35% and 23% of the sites were sources in the Rockies for CO_2 and CH_4, respectively.

Significant differences emerged between stream orders for pCO_2 (repeated measures ANOVA, n = 449, $f_{3,140}$ = 29.68, $P < 0.0001$) and pCH_4 (repeated measures ANOVA, n = 449, $f_{3,140}$ = 24.93, $P < 0.0001$). Significant differences between stream order 5 and other orders for both gases emerged, even after controlling for sample size (Figure 4) (Tukey's, $\alpha < 0.05$). Interestingly, the standard deviation were highest for pCO_2 in the lowest order streams with the opposite being true for pCH_4 (Table S3). For pCH_4, the highest variability could be found in the higher-order sections once the stream had entered into the lowlands.

We found significant differences between the means of carbonate versus noncarbonate sites for pCO_2 (WT, n = 449, $t_{5,\ 95}$ = 4.0557, $P < 0.0001$) and pCH_4 (WT, n = 449, $t_{5,\ 95}$ = 5.87, $P < 0.0001$). Areas with underlying carbonate lithology (>0% carbonates; Table S1) had 1.8 μatm pCH_4 and 22 μatm pCO_2 higher concentrations. The presence of agriculture (% agricultural area > 0) surfaced as a significant factor explaining variability for pCO_2 (WT, n = 449, $t_{5,95}$ = 11.59, $P < 0.0001$) and pCH_4 (WT, n = 449, $t_{5,\ 95}$ = 11.98, $P < 0.0001$). Sites with agricultural land use (Table 1) had 178 and 3.7 μatm higher pCO_2 and pCH_4, respectively. Interestingly, pCH_4 showed a significant difference between sites with urban development (Table S1). (WT, n = 449, $t_{5,\ 95}$ = 8.23, $P < 0.0001$) as did pCO_2 (WT, n = 449, $t_{5,\ 95}$ = 7.8, $P < 0.0001$). Sampled reaches with urban development, defined as satellite detection of any impervious surface area > 0, had 100 μatm higher mean pCO_2 and 1.9 μatm higher mean pCH_4 than watersheds with no impervious surface from development. The National Wetland Inventories wetland area estimates, expressed as a percent of subbasin area (Table 1), were a significant predictor for pCH_4 (WT, n = 449, $t_{5,\ 95}$ = 6.522, $P < 0.0001$) and pCO_2 (WT, n = 449, $t_{5,\ 95}$ = 7.57, $P < 0.0001$). Sites with wetland presence (>0% wetland area) had 102 μatm higher mean pCO_2 values and 2.2 μatm more pCH_4 than those without wetlands.

3.5. Temporal Variability

We observed significant temporal variability in partial pressures for pCO_2 (repeated measures ANOVA, n = 449, $f_{24,228}$ = 28.08, $p < 0.0001$) and pCH_4 (repeated measures ANOVA, n = 449, $f_{24,228}$ = 4.592, $p < 0.0001$) between the six sampling dates for the longitudinal data set (Figure 3). Streams were above atmospheric equilibration for both gases. This saturation was not consistent (Figure 3). Observations dropped as low as 114 μatm for pCO_2 and 0.13 μatm for pCH_4 during different points of our sampling period (n = 449). Lower elevation sites (1–8) show higher gas fluxes across all dates. In mid-July the distribution of the samples changes as more outliers emerge outside the interquartile range (Figure 3). The highest average network concentrations for pCO_2 along the longitudinal transect (n = 449) was observed in mid-July for pCO_2 (524 μatm) and 1 July for pCH_4 (2.6 μatm). Similar to pCO_2, average saturation of pCH_4 increased with decreasing flow in the early summer with a peak in mid-July. During early August, pCH_4 was remarkably uniformly low in the upper elevation and higher in the lower sites (Figure 3). pCH_4 rose again in late October. Like

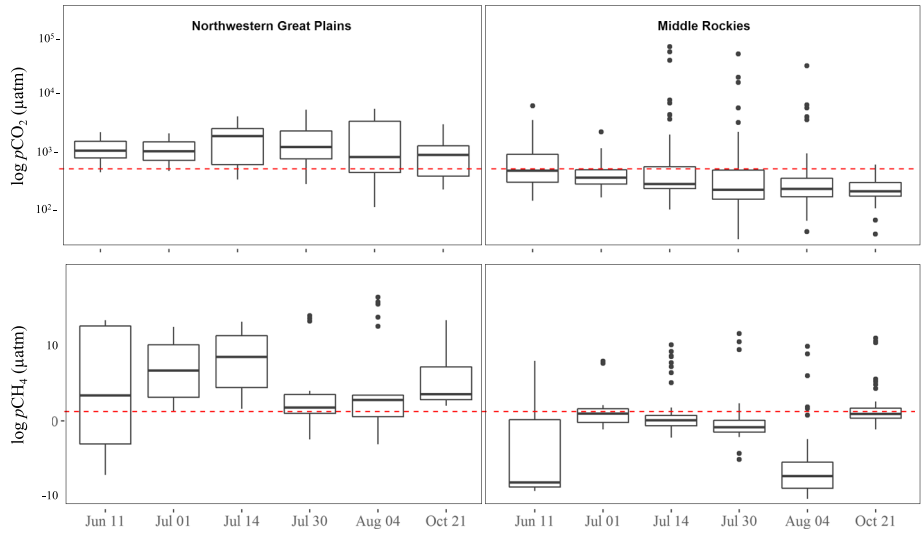

Figure 3. Boxplots showing the median (thick horizontal center line), first and third quartiles (upper and lower horizontal bounds of box), and spread for both gases (vertical lines and dots) across the sampling period averaged for (left) the Plains and (right) the Middle Rockies ($n = 449$). Data are shown with a log transformation for ease of interpretation. The red lines indicate the atmospheric concentration for each gas. Untransformed version of this plot can be found in Figure S1.

pCO_2, the greatest individual pCH_4 recordings were observed in mid-July to early August, when flows were still high yet receding (18 m^3 s^{-1}) and stream temperatures had begun to increase (10.6°C).

In this higher temporal resolution data set differences emerged between the snowmelt and base flow period for fluxes but less so for partial pressures (n = 253). Gas concentrations for both gases were higher during base flow (n = 253) by 102 ppm pCO_2 and 1.3 ppm pCH_4, but these differences were barely significant (WT, n = 253, $t_{5,\ 95} = -2.0738$, P = 0.04 for pCO_2) for pCO_2 and not significant for pCH_4 (WT, n = 253, $t_{5,\ 95} = -1.6747$, P = 0.095 for pCH_4).

We found a significant difference in fluxes of CO_2 and CH_4 between snowmelt period (conservatively defined as all samples collected before 20 July) and base flow conditions (Figure 6). Average FCO_2 during snowmelt was 346 mmol m^{-2} d^{-1} and only 203 mmol m^{-2} d^{-1} during the base flow period (WT, $n = 253$, $t_{5,\ 95} = 4.2757$, $P < 0.0001$). FCH_4 followed a similar pattern with fluxes during snowmelt average 10.30 mmol m^{-2} d^{-1} and with base flow fluxes of 6.5 mmol m^{-2} d^{-1} (WT, $n = 253$, $t_{5,\ 95} = 4.5427$, $P = < 0.0001$). Interestingly, the standard deviation almost doubled from 121 mmol m^{-2} d^{-1} during the snowmelt pulse to 253 mmol m^{-2} d^{-1} FCO_2 in the late summer. FCH_4 also showed an increase in variability as the standard deviation dropped from 6.9 mmol m^{-2} d^{-1} to 2.4 mmol m^{-2} d^{-1} from the snowmelt to the base flow conditions.

4. Discussion

4.1. Contrasting Gas Concentration Dynamics in Great Plains and Rockies

Our data demonstrate that the Clear Creek fluvial network exhibits both supersaturation and undersaturation with pCH_4 and pCO_2 with respect to the atmosphere. Many studies of temperate and boreal systems, including those specific to the American West, show a gradual decline in partial pressures of pCH_4 and pCO_2 along the river continuum [*Raymond et al.*, 2012] as streams lose their high connectivity to supersaturated groundwater flow paths [*Hotchkiss et al.*, 2015] and increase their catchment area [*Humborg et al.*, 2010; *Crawford et al.*, 2013]. While we expected the uppermost headwaters in the Rockies to be consistently supersaturated with gases relative to the atmosphere, we, in fact, observed undersaturation. The Middle Rockies contained the majority of measured "not spots" or observations of undersaturation. Eighty-nine percent of the observations of undersaturation for CO_2 and 94% for CH_4 were from the headwater Middle Rockies sites (Table 3). Higher pCO_2 and pCH_4 surprisingly appeared downstream in the higher stream orders of the Great Plains (Figure 5). Relative to other systems, the magnitude of our estimates for the partial pressure of CO_2 (539 µatm) is much less than the recent global average estimate of 2400 µatm [*Lauerwald et al.*, 2015]. *Stanley et al.* [2015]

also documented lower pCH_4 concentrations in mountainous regions relative to other biomes [*Stanley et al*., 2015]. pCO_2 concentrations here are well below those documented in tropical [*Johnson et al*., 2008; *Wit et al*., 2015], temperate [*Jones and Mulholland*, 1998], and boreal systems [*Campeau et al*., 2014; *Kokic et al*., 2015; *Leith et al*., 2015]. The near-equilibrium concentration of gases observed in the Rockies surprisingly fails to support the commonly held hypothesis that headwater streams are consistently supersaturated with CO_2 and CH_4 [*Cole et al*., 2007; *Jones et al*., 2003] relative to the atmosphere.

4.2. Mountainous Sites Exhibit High sVariability and Undersaturation

Dissolved gas concentrations in the alpine Middle Rockies sites were low and highly variable (Figure 3), which could be due to a lack of carbonate buffering [*Stets et al*., 2017]. Our findings show agreement with *Crawford et al*. [2015], who found an average pCO_2 of 470 μatm and 3.5 μatm for pCH_4 for streams in the Colorado Rockies. Substrate limitation of terrestrially derived matter, which is thought to fuel aquatic carbon evasion, can be observed in shallow, acidic alpine soils whose carbon stocks are lower due to relatively lower rates of terrestrial productivity. Short growing seasons and cold stream temperatures (mean = 8°C) could slow the internal production of biogenic CO_2. The low pCO_2 and pCH_4 concentrations observed here could indicate minimal downstream greenhouse gas transport to lower sections of the network.

Wetland-associated alpine sites (>0%) showed higher concentrations than sites with no wetland coverage (0%) in some but not all cases. Alpine and subalpine, low-slope wetland complexes are also known to influence gas concentrations [*Wickland et al*., 1999; *Smith and Lewis*, 1992]. Our study area contained over 1.17 km^2 of freshwater emergent, shrub, and forested wetlands, and two wetland-adjacent sites, Brook Trout and Thousandth Bite (Table 2), did have pCO_2 values in the upper quartile of the distribution, but at Brook Trout, high pCO_2 values are not matched by a simultaneous increase in pCH_4. Furthermore, wetland % coverage did not correlate with elevated stream pCO_2 or pCH_4 concentrations (Table 2). For example, the subbasin drained by the Soldier Graves site has the largest percent wetland coverage (13.4%) with elevated pCH_4 levels (6.1 μatm) but pCO_2 (397 μatm) only slightly above saturation. Results could be conflicting because of the proximity of the wetlands to stream channel varied from site to site. Thus, it is possible wetland coverage and connectivity influence gas concentrations, but our data show that wetland coverage alone cannot explain the variability across all sites.

4.3. Great Plains Sites Exhibit Systemic Supersaturation

Contrary to most headwater stream studies [*Leith et al*., 2015; *Dinsmore et al*., 2013; *Kokic et al*., 2015; *Johnson et al*., 2008; *Palmer et al*., 2001; *Bishop et al*., 2008], concentrations and fluxes of CO_2 and CH_4 increased in the downstream Great Plains relative to the alpine headwaters. In the Great Plains, the deep, loamy well-drained floodplain soils house relatively higher carbon stocks [*Sams et al*., 2014] available for microbial greenhouse gas production. In addition, lower stream power, longer groundwater flow paths, and warmer temperatures (Table 2) can contribute to methanogenesis [*Sanders et al*., 2007]. Research by *Neumann et al*. [2010] in Bangladesh shows that groundwater recharge waters from constructed ponds can carry high loads of methane. Storage ponds dot the watershed, and the landscape is crisscrossed with over 572.8 km of irrigation canals and other artificial conveyance infrastructures (NHDPlus). Even though agricultural land use accounts for <0.1% of the total land cover in these semiarid rangelands [*Knight et al*., 2014] (Table S1), much of this development (Figure 1d) is constrained to riparian areas [*BLM*, 2006], thus having a larger impact on stream dynamics than their small landscape footprint might suggest.

Higher pH's and carbonate buffering in the Plains ecosystem could offset CO_2 production and uncouple CO_2 and CH_4 dynamics. This is supported by the significant difference we found for pCO2 between carbonate and noncarbonate sites. While the higher pH observed in the Great Plains may lower CO_2 concentrations relative to ${CO_2}^{2-}$ and ${HCO_3}^{-}$ [*Wetzel*, 2001], nutrient and organic matter-rich return water from irrigated fields could alternately boost instream respiration, enhancing CO_2 contributions from metabolism [*Tilman et al*., 2002]. Crop production and intensive grazing in riparian zones can lead to cattle-vectorized allochthonous organic matter loading [*Carpenter et al*., 1998; *Conroy et al*., 2016] which could accelerate carbon cycling [*Guenet et al*., 2010]. Further research into the age of carbon fractions and stream metabolism could reveal the relative geologic and biological influences at play in this system.

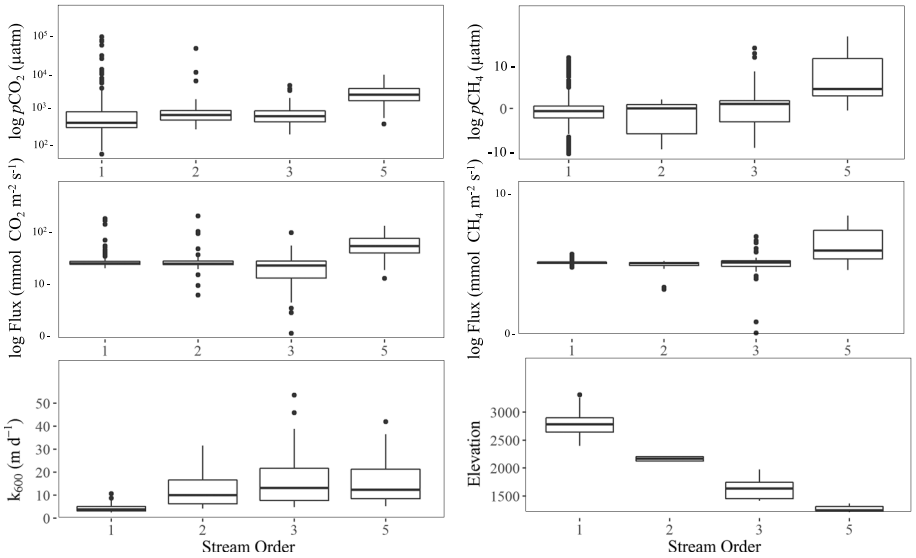

Figure 4. Boxplots showing the median (thick horizontal center line), first and third quartiles (upper and lower horizontal bounds of box) for dissolved gas concentrations, and fluxes and estimated k_{600} across stream orders (n = 449). The decrease in elevation across stream orders is shown in the bottom right plot for reference for each stream order. Data are shown with a log transformation for ease of interpretation. Before transformation, fluxes were scaled using a constant (minimum flux +0.0001) to ensure the inclusion of negative values. Untransformed version of this plot can be found in Figure S2.

While an investigation of these individual processes is not within the scope of this paper, a similar pattern of increasing pCH_4 concentrations along a downstream gradient has been observed in rivers of the Pacific Northwest, USA, and is thought to be due to accumulating inputs from forested and agricultural catchments [*De Angelis and Lilley*, 1987]. Our results show the potential for shifts in greenhouse gas fluxes when moving along a gradient from steeper regions with thinner soils to lowland regions. This shift may also be impacted by human land use practices and changes in equilibration rates due to increased pH and carbonate buffering [*Regnier et al*., 2013; *Stets et al*., 2017]. Research has shown that agricultural intensification [*Samson et al*., 2004] has altered terrestrial net greenhouse gas exchange for the Plains [*Hartman et al*., 2011]. Ecological and human-induced land use/land cover as a driver has been shown before for other aquatic systems [e.g., *Bodmer et al*., 2016; *Lapierre et al*., 2013], but their relative weight here remains unknown and could benefit from a more integrated conceptual framework, such as that offered for lakes and reservoirs by *Hayes et al*. [2017].

4.4. Changes Associated With Snowmelt and Baseflow

Studies from diverse systems cite shydrology as a first-order control on efflux from aquatic conduits [*Richey et al*., 2002; *Long et al*., 2015], and the high discharge associated with snowmelt events can be responsible for large proportions of carbon transport (pulses) into streams [*Raymond et al*., 2016]. Our data show that spring high flows (Figure 2) are associated with supersaturated gas concentrations (Figure 3) and high k's due to high turbulence. These conditions bring a system-wide pulse of gas (Figure 6) despite cold stream temperatures, low light penetration, and dilution of constituents during high discharge. FCO_2 and FCH_4 during the descending limb of spring runoff are 44% and 58% higher for (Figure 6) than those taken during base flow conditions of mid to late-summer (n = 253). These results agree with other studies documenting pulses of pCO_2 during runoff peaks in both headwater streams [*Leith et al*., 2015; *Kokic et al*., 2015; *Dinsmore et al*., 2013] and larger systems [*Richey et al*., 2002]. While our calculations of snowmelt contributions are likely conservative as the stream could only be safely sampled on the descending limb of snowmelt, these findings support our conclusion that snowmelt-driven fluxes can provide an under-accounted yet large percent of greenhouse gas fluxes at annual scales.

During base flow, CO_2 and CH_4 fluxes exhibit divergent seasonal and spatial trends. Interestingly, while system-wide concentrations are higher during snowmelt, periods of low flow show the development of ephemeral hot spots of methane saturation (Figure 3) and evasion (Figure 4). Studies from very different systems in West Africa [*Koné et al*., 2010] and the Amazon [*Sawakuchi et al*., 2014] show increases in CH_4 fluxes

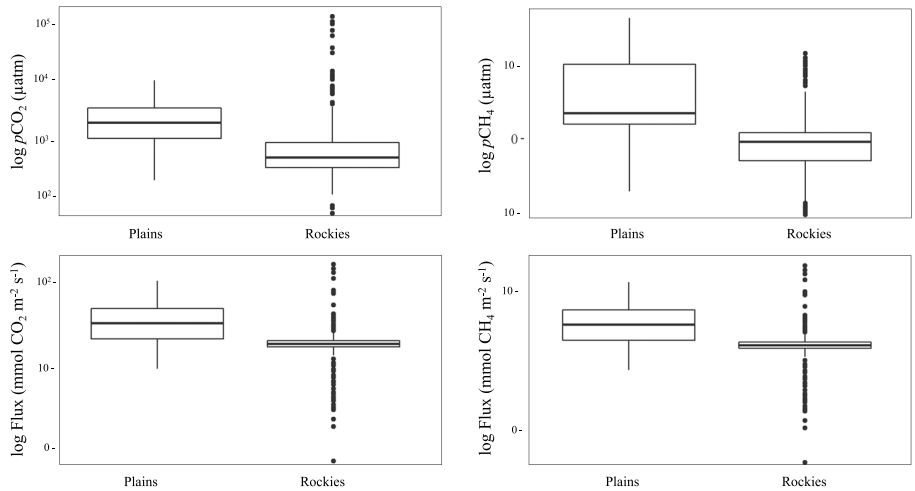

Figure 5. Boxplots showing log-transformed saturation values for each gas by ecoregion (Plains = 1, Rockies = 2) across all sampling dates (n = 449). Medians, means, and variability can be found in Table 3. Data are shown with a log transformation for ease of interpretation. Before transformation, fluxes were scaled using a constant (minimum flux +0.0001) to ensure the inclusion of negative values. Untransformed version of this plot can be found in Figure S3.

during periods of low flow, when warmer stream temperatures can enhance microbial processing rates. Unlike pCH_4, pCO_2 remained surprisingly low throughout the late summer (Figure 3), a time when warm temperatures and slower flow have been shown to support net heterotrophy in boreal systems [*Öquist et al.*, 2009] but may instead, coupled with lower turbidity, contribute to enhance primary productivity here. For extended investigation into the geochemical and ecological changes during base flow, see Text S1 in the supporting information. Of the few observations in which the Great Plains sites acted as a pCO_2 sinks, 98% occurred after the onset of summer base flow (n = 449). Interestingly, variability tended to increase for both gases during the initiation of the low-flow period around mid-July (Figure 3), as ephemeral hot spots of gas flux emerged during late summer (n = 449). Based on the larger number of values outside the interquartile range observed during base flow, we caution the use of small sample sizes for scaling from watersheds of this type and encourage the collection of robust spatiotemporal survey data. Data from this study had the largest spread in the lowest stream orders sampled in the summer, suggesting that surveys conducted during base flow with only a few samples could easily misrepresent the distribution of the data.

4.5. Implications for Regional Gas Evasion

Our average flux estimates (107 mmol m^{-2} d^{-1}, range = −125 to 566 mmol m^{-2} d^{-1}) for CO_2 are comparable to the regional estimates for the West by *Butman and Raymond* [2011] of 70.34 mmol CO_2 m^2 d^{-1} but are higher than the only other published study for the Rockies [*Crawford et al.*, 2015) that measured FCO_2 at 35.9 mmol m^2 d^{-1} using instantaneous flux methods (n = 702). Since our data set had a larger elevation range, for a more direct comparison we subset our data set to the elevation range (2780 m–3505 m) in *Crawford et al.* [2015]. This gives a substantially lower estimate of flux (4.7 mmol m^2 d^{-1}). Even with the large uncertainties associated with empirically estimating flux, gas evasion reported by this study and *Crawford et al.* [2015] suggests that regional flux estimates for the Rockies are currently overestimating fluxes in this mountainous region.

Mean methane efflux (2.4 mmol m^{-2} d^{-1}, range = −1.2 to 48 mmol m^{-2} d^{-1}) was low compared with the worldwide mean reported value of 8.22 mmol m^{-2} d^{-1} from a global survey of 385 lakes by *Stanley et al.* [2015] but fell within the range reported both by that study and the range for FCH_4 from the Colorado Rockies study (n = 702) [*Crawford et al.*, 2015; *Stanley et al.*, 2015]. Lower FCH_4 observed in the forested, wilderness sites (Figures 5 and 6) found in the Middle Rockies could be due to either reduced substrate availability, higher methane oxidation rates, or potentially atmospheric deposition of sulfate (see Text S2 for extended discussion).

While emissions from this system are lower than regional averages for other ecosystems [*Stanley et al.*, 2015; *Butman et al.*, 2016; *Call et al.*, 2015; *Sand-Jensen and Staehr*, 2012; *Jones and Mulholland*, 1998], the contrast

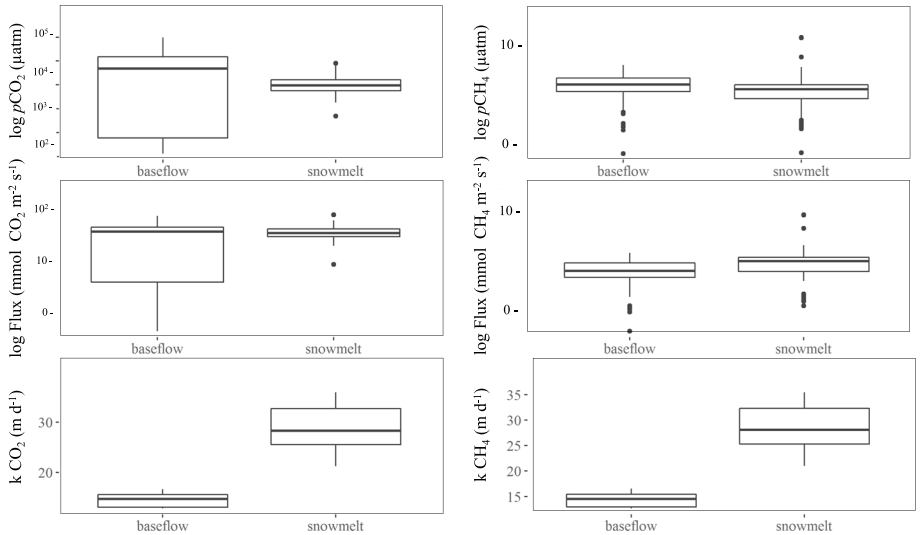

Figure 6. Boxplots showing the log-transformed flux with a constant (minimum flux +0.0001) added and concentration during snowmelt (11 June (first sampling date) to 20 July) and after the freshet has passed (20 July onward) (n = 253). Gas transfer velocities are not transformed. Untransformed version of this plot can be found in Figure S4.

between ecoregions is an important finding (Figure 3), suggesting that landscape scale changes can be used to inform our understanding of trends in carbon dynamics. These larger spatial patterns, however, are countered by high local heterogeneity within each site and sampling run (Figure 3 and Table 2). The presence of small, seasonal hot spots, especially in agricultural areas and around wetlands, could be of importance. In addition, the relatively high FCH_4 from semiarid agricultural areas suggest that the inland waters of the Great Plains could contribute more methane than expected to regional greenhouse gas budgets.

However, the fluxes calculated here are associated with high uncertainty, especially for systems bordering equilibrium. Despite the high elevations, hydraulic geometry coefficients may underestimate stream surface area and flux because of the extensive braiding common in the large, high-elevation meadows [*Livers and Wohl*, 2016]. More detailed field studies, particularly using comparative flux measurement techniques, are recommended to constrain uncertainty in flux estimates.

We also recognize that our data set is biased toward daytime and summertime measurements, which can lead to an overestimation of diel fluxes [*Baulch et al*., 2012; *Schelker et al*., 2016; *Peter et al*., 2014]. Furthermore, we were not able to constrain total flux of methane. Our sampling was restricted solely to diffusive flux, while up to 90% of methane flux can be mediated by plants and through ebullition (i.e., bubbles) [*Likens*, 2010; *Sawakuchi et al*., 2014; *Bhullar et al*., 2013]. In addition, the assumption of zero emissions during the ice season could underestimate total flux [*Campeau et al*., 2014]. Several studies highlight winter as a time of high partial pressures and evasion [*Crawford et al*., 2015, *Jones and Mulholland*, 1998], but as no data on gas dynamics under ice cover exists for this system our numbers represent a conservative estimate. Given these uncertainties, our estimates are probably lower than if they had been taken using flux chambers, in part because chambers can lead to overestimated fluxes by changing turbulence, pressure, and temperature at the water-air interface [*Marx et al*., 2017]. These considerations highlight the need for higher-resolution time series of in situ comparative flux measurements to achieve closure between these methods. Long-term studies conducted throughout the year, such as in *Atkins et al*. [2016], and across a range of annual discharges will no doubt bring to light new insights into these processes.

5. Conclusions

This study provides initial measurements of CO_2 and methane for an understudied region, filling in an important geographic and altitudinal gap and providing a counterpoint to the commonly held assumption that headwater streams are supersaturated relative to the atmosphere. We find significantly higher

concentrations and fluxes for CO_2 and CH_4 in the agricultural-impacted Great Plains region relative to its alpine headwaters, suggesting that fluxes for alpine areas, as well as their contribution to downstream gas loading, may currently be overestimated. Our study also investigates the impact of snowmelt on carbon gas dynamics. Our results suggest that the relationship between fluxes and discharge could be sensitive to hydrologic shifts associated with changing rain-snow ratios [*Foster et al*., 2016]. Many studies forecast an increase in winter runoff, earlier and faster snowmelt, and a decrease in summer runoff [*Najafi and Moradkhani*, 2015; *Hall et al*., 2015; *Wolock and McCabe*, 1999], but it remains unclear how changes in hydrologic variability may alter fluxes. Understanding the impact of landscape diversity and climate conditions on aquatic C fluxes is crucial to reducing uncertainty associated with scaling carbon budgets for inland waters on regional and global scales.

Acknowledgments
Funding for this work came from the Ucross High Plains Stewardship Initiative with additional support from the Yale Institute for Biospheric Studies, Yale School of Forestry Carpenter Sperry, and Jubitz Research Funding. Many people made this sampling possible, so thanks to the Ucross Foundation, Apache Foundation, Merlin Ranch, Victoria Station Ranch, Buffalo City Water Treatment Plant, Chris at States West, Cheryl and Tina at Steady Stream Hydrology, and the U.S. Forest Service at the Bighorn National Forest. Thanks to Bridger Konkel, and Kris Covey for field and lab support and to Matt Bogard and the anonymous reviewers for their constructive feedback. Thanks to Andy Tuller, Ruby, and everyone in the Raymond Saiers Lab. All data discussed in this publication appear in the figures, text, tables, and supporting information of this publication. This manuscript is dedicated to Heather West.

References

Abril, G., et al. (2015), Large overestimation of pCO_2 calculated from pH and alkalinity in acidic, organic-rich freshwaters, *Biogeosciences*, *12*(1), 67–78.

Ågren, A., M. Haei, S. Köhler, K. Bishop, and H. Laudon (2010), Long cold winters give higher stream water dissolved organic carbon (DOC) concentrations during snowmelt, *Biogeosci. Discuss.*, *7*(3), 4857–4886.

Algesten, G., S. Sobek, A.-K. Bergström, A. Ågren, L. J. Tranvik, and M. Jansson (2004), Role of lakes for organic carbon cycling in the boreal zone, *Global. Change Biol.*, *10*(1), 141–147.

Allan, J. D. (2004), Landscapes and riverscapes: The influence of land use on stream ecosystems, *Annu. Rev. Ecol. Evol. Syst.*, *35*(1), 257–284, doi:10.1146/annurev.ecolsys.35.120202.110122.

Atkins, M. L., I. R. Santos, and D. T. Maher (2016), Seasonal exports and drivers of dissolved inorganic and organic carbon, carbon dioxide, methane and δ13C signatures in a subtropical river network, *Sci. Total Environ.*, *575*, 545–563.

Aufdenkampe, A. K., E. Mayorga, P. A. Raymond, J. M. Melack, S. C. Doney, S. R. Alin, R. E. Aalto, and K. Yoo (2011), Riverine coupling of biogeochemical cycles between land, oceans, and atmosphere, *Front. Ecol. Environ.*, *9*(1), 53–60, doi:10.1890/100014.

Barnes, R. T., and P. A. Raymond (2009), The contribution of agricultural and urban activities to inorganic carbon fluxes within temperate watersheds, *Chem. Geol.*, *266*(3–4), 318–327.

Bastviken, D., et al. (2011), Freshwater methane emissions offset the continental carbon sink, *Science*, *331*(6013), 50.

Baulch, H. M., P. J. Dillon, R. Maranger, J. J. Venkiteswaran, H. F. Wilson, and S. L. Schiff (2012), Night and day: Short-term variation in nitrogen chemistry and nitrous oxide emissions from streams, *Freshw. Biol.*, *57*(3), 509–525, doi:10.1111/j.1365-2427.2011.02720.x.

Bhullar, G. S., et al. (2013), Methane transport and emissions from soil as affected by water table and vascular plants, *BMC Ecol.*, *13*, 32.

Bishop, K., I. Buffam, M. Erlandsson, J. Fölster, H. Laudon, J. Seibert, and J. Temnerud (2008), Aqua incognita: The unknown headwaters, *Hydrol. Process.*, *22*(8), 1239–1242.

BLM (2002), *Final Environmental Impact Statement and Proposed Plan Amendment for the Powder River Basin Oil and Gas Project*, Buffalo Field Office, Wyo.

BLM (2006), Water resources of the Wyoming Powder River Basin. [Available at http://www.blm.gov/pgdata/etc/medialib/blm/wy/programs/energy/coal/prb/coalreview/task1b.Par.47799.File.dat/ch3.pdf.]

Bodmer, P., M. Heinz, M. Pusch, G. Singer, and K. Premke (2016), Carbon dynamics and their link to dissolved organic matter quality across contrasting stream ecosystems, *Sci. Total Environ.*, *553*, 574–586.

Borges, A. V., et al. (2015), Globally significant greenhouse gas emissions from African inland waters, *Nat. Geosci.*, *8*(8), 637–642.

Butman, D., and P. A. Raymond (2011), Significant efflux of carbon dioxide from streams and rivers in the United States, *Nat. Geosci.*, *4*(12), 839–842, doi:10.1038/ngeo1294.

Butman, D., S. Stackpoole, E. Stets, C. P. McDonald, D. W. Clow, and R. G. Striegla (2016), Aquatic carbon cycling in the conterminous United States and implications for terrestrial carbon accounting, *Proc. Natl. Acad. Sci. U.S.A.*, *113*(1), 58–63.

Butman, D. E., H. F. Wilson, R. T. Barnes, M. A. Xenopoulos, and P. A. Raymond (2014), Increased mobilization of aged carbon to rivers by human disturbance, *Nat. Geosci.*, *8*(2), 112–116.

Call, M., et al. (2015), Spatial and temporal variability of carbon dioxide and methane fluxes over semi-diurnal and spring–neap–spring timescales in a mangrove creek, *Geochim. Cosmochim. Acta*, *150*, 211–225.

Campbell, D. H., D. W. Clow, G. P. Ingersoll, M. A. Mast, N. E. Spahr, and J. T. Turk (1995), Processes controlling the chemistry of two snowmelt-dominated streams in the Rocky Mountains, *Water Resour. Res.*, *31*, 2811–2821.

Campeau, A., and P. A. Del Giorgio (2014), Patterns in CH4 and CO2 concentrations across boreal rivers: Major drivers and implications for fluvial greenhouse emissions under climate change scenarios, *Global Change Biol.*, *20*(4), 1075–1088.

Campeau, A., J.-F. Lapierre, D. Vachon, and P. A. del Giorgio (2014), Regional contribution of CO_2 and CH_4 fluxes from the fluvial network in a lowland boreal landscape of Québec, *Global Biogeochem. Cycles*, *28*, 57–69, doi:10.1002/2013GB004685.

Carey, J. C., and R. W. Fulweiler (2012), Human activities directly alter watershed dissolved silica fluxes, *Biogeochemistry*, *111*(1), 125–138, doi:10.1007/s10533-011-9671-2.

Carpenter, S. R., et al. (1998), Nonpoint pollution of surface waters with phosphorus and nitrogen, *Ecol. Appl.*, *8*(3), 559–568, doi:10.1890/1051-0761(1998)008[0559:NPOSWW]2.0.CO;2.

Cayan, D. R., M. D. Dettinger, D. Pierce, T. Das, N. Knowles, F. M. Ralph, and E. Sumargo (2016), Natural variability, anthropogenic climate change and impacts on water availability and flood extremes in the western United States, in *Chapter 2 in Western Water Policy & Planning in a Variable & Changing Climate*, edited by K. Miller, pp. 17–42, CRC Press, a Taylor & Francis Group, Boca Raton, Fla.

Climate, O.W.S. (2016), *Water Resources Data System*, Laramie, Wyu. [Available at http://www.wrds.uwyo.edu/sco/data/datamap.html.]

Cole, J. J., et al. (2007), Plumbing the global carbon cycle: Integrating inland waters into the terrestrial carbon budget, *Ecosystems*, *10*(1), 172–185, doi:10.1007/s10021-006-9013-8.

Conroy, E., J. N. Turner, A. Rymszewicz, J. J. O'Sullivan, M. Bruen, D. Lawler, H. Lally, and M. Kelly-Quinn (2016), The impact of cattle access on ecological water quality in streams: Examples from agricultural catchments within Ireland, *Sci. Total Environ.*, *547*, 17–29.

Crawford, J. T., R. G. Striegl, K. P. Wickland, M. M. Dornblaser, and E. H. Stanley (2013), Emissions of carbon dioxide and methane from a headwater stream network of interior Alaska, *J. Geophys. Res. Biogeosci.*, *118*, 482–494, doi:10.1002/jgrg.20034.

Crawford, J. T., M. M. Dornblaser, E. H. Stanley, D. W. Clow, and R. G. Striegl (2015), Source limitation of carbon gas emissions in high-elevation mountain streams and lakes, *J. Geophys. Res. Biogeosci.*, *120*, 952–964, doi:10.1002/2014JG002861.

D'Amario, S. C., and M. A. Xenopoulos (2015), Linking dissolved carbon dioxide to dissolved organic matter quality in streams, *Biogeochemistry*, *126*(1–2), 99–114, doi:10.1007/s10533-015-0143-y.

David, G. C. L., E. Wohl, S. E. Yochum, and B. P. Bledsoe (2010), Controls on at-a-station hydraulic geometry in steep headwater streams, Colorado, USA, *Earth Surf. Process. Landf.*, *35*(15), 1820–1837, doi:10.1002/esp.2023.

Dawson, J. J. C., C. Soulsby, D. Tetzlaff, M. Hrachowitz, S. M. Dunn, and I. A. Malcolm (2008), Influence of hydrology and seasonality on DOC exports from three contrasting upland catchments, *Biogeochemistry*, *90*(1), 93–113, doi:10.1007/s10533-008-9234-3.

De Angelis, M. A., and M. D. Lilley (1987), Methane in surface waters of Oregon estuaries and rivers, *Limnol. Oceanogr.*, *32*(3), 716–722, doi:10.4319/lo.1987.32.3.0716.

Dinsmore, K. J., and M. F. Billett (2008), Continuous measurement and modeling of CO2 losses from a peatland stream during stormflow events, *Water Resour. Res.*, *44*, W12417, doi:10.1029/2008WR007284.

Dinsmore, K. J., M. B. Wallin, M. S. Johnson, M. F. Billett, K. Bishop, J. Pumpanen, and A. Ojala (2013), Contrasting CO_2 concentration discharge dynamics in headwater streams: A multi-catchment comparison, *J. Geophys. Res. Biogeosci.*, *118*, 445–461, doi:10.1002/jgrg.20047.

Dise, N. B., and E. S. Verry (2001), Suppression of peatland methane emission by cumulative sulfate deposition in simulated acid rain, *Biogeochemistry*, *53*(2), 143–160.

Doherty, K. E., D. E. Naugle, B. L. Walker, and J. M. Graham (2008), Greater sage-grouse winter habitat selection and energy development, *J. Wildl. Manage*, *72*(1), 187–195, doi:10.2193/2006-454.

Dürr, H. H., M. Meybeck, and S. H. Dürr (2005), Lithologic composition of the Earth's continental surfaces derived from a new digital map emphasizing riverine material transfer, *Global Biogeochem. Cycles*, *19*, GB4S10, doi:10.1029/2005GB002515.

Environmental Systems Research Institute Inc (2008), ArcGIS—A complete integrated system.

Finlay, J. C. (2003), Controls of streamwater dissolved inorganic carbon dynamics in a forested watershed, *Biogeochemistry*, *62*(3), 231–252, doi:10.1023/A%253A1021183023963.

Foster, L. M., L. A. Bearup, N. P. Molotch, P. D. Brooks, and R. M. Maxwell (2016), Energy budget increases reduce mean streamflow more than snow–rain transitions: Using integrated modeling to isolate climate change impacts on Rocky Mountain hydrology, *Environ. Res. Lett.*, *11*(4), 44015.

Fox, J., and S. Weisberg (2011), *An {R} Companion to Applied Regression*, 2nd ed., Sage, Thousand Oaks, Calif. [Available at http://socserv.socsci.mcmaster.ca/jfox/Books/Companion.]

Fry, J. A., et al. (2011), Completion of the 2006 national land cover database for the conterminous United States, *Photogramm. Eng. Remote. Sens.*, *77*(9), 858–864.

Gauci, V., et al. (2004), Sulfur pollution suppression of the wetland methane source in the 20th and 21st centuries, *Proc. Natl. Acad. Sci. U.S.A.*, *101*(34), 12,583–12,587.

Genereux, D. P., and H. F. Hemond (1992), Determination of gas exchange rate constants for a small stream on Walker Branch Watershed, Tennessee, *Water Resour. Res.*, *28*, 2365–2374, doi:10.1029/92WR01083.

Gesch, D., et al. (2002), The national elevation dataset, *Photogramm. Eng. Remote. Sens.*, *68*(1), 5–32.

Guenet, B., M. Danger, L. Abbadie, and G. Lacroix (2010), Priming effect: Bridging the gap between terrestrial and aquatic ecology, *Ecology*, *91*(10), 2850–2861, doi:10.1890/09-1968.1.

Hall, D. K., C. J. Crawford, N. E. DiGirolamo, G. A. Riggs, and J. L. Foster (2015), Detection of earlier snowmelt in the Wind River Range, Wyoming, using Landsat imagery, 1972–2013, *Remote Sens. Environ.*, *162*, 45–54.

Hartman, M. D., E. R. Merchant, W. J. Parton, M. P. Gutmann, S. M. Lutz, and S. A. Williams (2011), Impact of historical land-use changes on greenhouse gas exchange in the US Great Plains, 1883–2003, *Ecol. Appl.*, *21*(4), 1105–1119.

Hayes, N. M., B. R. Deemer, J. R. Corman, N. R. Razavi, and K. E. Strock (2017), Key differences between lakes and reservoirs modify climate signals: A case for a new conceptual model, *Limnol. Oceanogr. Lett.*, *2*(2), 47–62.

Hope, D., J. J. C. Dawson, M. S. Cresser, and M. Billett (1995), A method for measuring free CO_2 in upland streamwater using headspace analysis, *J. Hydrol.*, *166*(1), 1–14.

Hope, D., S. M. Palmer, M. F. Billett, and J. J. C. Dawson (2004), Variations in dissolved CO_2 and CH_4 in a first-order stream and catchment: An investigation of soil–stream linkages, *Hydrol. Process.*, *18*(17), 3255–3275.

Hotchkiss, E. R., et al. (2015), Sources of and processes controlling CO_2 emissions change with the size of streams and rivers, *Nat. Geosci.*, *8*(9), 696–699, doi:10.1038/ngeo2507.

Houghton, R. A., J. I. House, J. Pongratz, G. R. van der Werf, R. S. DeFries, M. C. Hansen, C. Le Quere, and N. Ramankutty (2012), Carbon emissions from land use and land-cover change, *Biogeosciences*, *9*(12), 5125–5142.

Humborg, C., C.-M. Mörth, M. Sundbom, H. Borg, T. Blenckner, R. Giesler, and V. Ittekkot (2010), CO_2 supersaturation along the aquatic conduit in Swedish watersheds as constrained by terrestrial respiration, aquatic respiration and weathering, *Global Change Biol.*, *16*(7), 1966–1978.

Jähne, B., G. Heinz, and W. Dietrich (1987), Measurement of the diffusion coefficients of sparingly soluble gases in water, *J. Geophys. Res.*, *92*, 10,767–10,776, doi:10.1029/JC092iC10p10767.

Johnson, M. S., et al. (2008), CO_2 efflux from Amazonian headwater streams represents a significant fate for deep soil respiration, *Geophys. Res. Lett.*, *35*, L17401, doi:10.1029/2008GL034619.

Jones, J., and P. Mulholland (1998), Carbon dioxide variation in a hardwood forest stream: An integrative measure of whole catchment soil respiration, *Ecosystems*, *1*(2), 183–196, doi:10.1007/s100219900014.

Jones, J. B., E. H. Stanley, and P. J. Mulholland (2003), Long-term decline in carbon dioxide supersaturation in rivers across the contiguous United States, *Geophys. Res. Lett.*, *30*(10), 1495, doi:10.1029/2003GL017056.

Kaushal, S. S., G. E. Likens, N. A. Jaworski, M. L. Pace, A. M. Sides, D. Seekell, K. T. Belt, D. H. Secor, and R. L. Wingate (2010), Rising stream and river temperatures in the United States, *Front. Ecol. Environ.*, *8*(9), 461–466.

Kling, G. W., G. W. Kipphut, and M. C. Miller (1991), Arctic lakes and streams as gas conduits to the atmosphere: Implications for tundra carbon budgets, *Science*, *251*(4991), 298.

Knight, D. H., et al. (2014), *Mountains and Plains: The Ecology of Wyoming Landscapes*, Yale Univ. Press, New Haven, Conn.

Kokic, J., M. B. Wallin, H. E. Chmiel, B. A. Denfeld, and S. Sobek (2015), Carbon dioxide evasion from headwater systems strongly contributes to the total export of carbon from a small boreal lake catchment, *J. Geophys. Res. Biogeosci.*, *120*, 13–28, doi:10.1002/2014JG002706.

Koné, Y. J. M., G. Abril, B. Delille, and A. V. Borges (2010), Seasonal variability of methane in the rivers and lagoons of Ivory Coast (West Africa), *Biogeochemistry*, *100*(1–3), 21–37.

Lapierre, J.-F., F. Guillemette, M. Berggren, and P. A. del Giorgio (2013), Increases in terrestrially derived carbon stimulate organic carbon processing and CO_2 emissions in boreal aquatic ecosystems, *Nat. Commun.*, *4*, 2972.

Lauerwald, R., G. G. Laruelle, J. Hartmann, P. Ciais, and P. A. Regnier (2015), Spatial patterns in CO_2 evasion from the global river network, *Global Biogeochem. Cycles*, *29*, 534–554, doi:10.1002/2014GB004941.

Leith, F. I., et al. (2015), Carbon dioxide transport across the hillslope-riparian-stream continuum in a boreal headwater catchment, *Biogeosciences*, *12*, 1881–1892.

Likens, G. (2010), *Biogeochemistry of Inland Waters*, Elsevier/Academic Press, Amsterdam, Boston.

Livers, B., and E. Wohl (2016), Sources and interpretation of channel complexity in forested subalpine streams of the Southern Rocky Mountains, *Water Resour. Res.*, *52*, 3910–3929, doi:10.1002/2015WR018306.

Logan, K. A., and L. L. Irwin (1985), Mountain lion habitats in the Big Horn Mountains, Wyoming, *Wildl. Soc. Bull.*, *13*(3), 257–262.

Long, H., et al. (2015), Hydraulics are a first order control on CO_2 efflux from fluvial systems, *J. Geophys. Res. Biogeosci.*, *120*, 1912–1922, doi:10.1002/2015JG002955.

Manahan, S. E. (1993), *Fundamentals of Environmental Chemistry*, Lewis Publ., Chelsea, Mich.

Mapel, W. J. (1959), *Geology and Coal Resources of the Buffalo-Lake de Smet Area, Johnson and Sheridan Counties*, U.S. Govt. Print. Office, Wyoming.

Marx, A., J. Dusek, J. Jankovec, M. Sanda, T. Vogel, R. van Geldern, J. Hartmann, and J. A. C. Barth (2017), A review of CO_2 and associated carbon dynamics in headwater streams: A global perspective, *Rev. Geophys.*, *55*, 560–585, doi:10.1002/2016RG000547.

Mayorga, E., A. K. Aufdenkampe, C. A. Masiello, A. V. Krusche, J. I. Hedges, P. D. Quay, J. E. Richey, and T. A. Brown (2005), Young organic matter as a source of carbon dioxide outgassing from Amazonian rivers, *Nature*, *436*(7050), 538–541.

McGinnis, D. F., G. Kirillin, K. W. Tang, S. Flury, P. Bodmer, C. Engelhardt, P. Casper, and H. P. Grossart (2015), Enhancing surface methane fluxes from an oligotrophic lake: Exploring the microbubble hypothesis, *Environ. Sci. Technol.*, *49*(2), 873–880, doi:10.1021/es503385d.

Mote, P. W., A. F. Hamlet, M. P. Clark, and D. P. Lettenmaier (2005), Declining mountain snowpack in western North America, *Bull. Am. Meteorol. Soc.*, *86*(1), 39.

Najafi, M. R., and H. Moradkhani (2015), Multi-model ensemble analysis of runoff extremes for climate change impact assessments, *J. Hydrol.*, *525*, 352–361.

Nanus, L., D. H. Campbell, G. P. Ingersoll, D. W. Clow, and M. A. Mast (2003), Atmospheric deposition maps for the Rocky Mountains, *Atmos. Environ.*, *37*(35), 4881–4892.

Neumann, R. B., K. N. Ashfaque, A. B. M. Badruzzaman, M. A. Ali, J. K. Shoemaker, and C. F. Harvey (2010), Anthropogenic influences on groundwater arsenic concentrations in Bangladesh, *Nat. Geosci.*, *3*(1), 46–52.

Öquist, M. G., M. Wallin, J. Seibert, K. Bishop, and H. Laudon (2009), Dissolved inorganic carbon export across the soil/stream interface and its fate in a boreal headwater stream, *Environ. Sci. Technol.*, *43*(19), 7364–7369, doi:10.1021/es900416h.

Oh, N., and P. A. Raymond (2006), Contribution of agricultural liming to riverine bicarbonate export and CO_2 sequestration in the Ohio River basin, *Global Biogeochem. Cycles*, *20*, GB3012, doi:10.1029/2005GB002565.

Palmer, S. M., D. Hope, M. F. Billett, J. J. C. Dawson, and C. L. Bryant (2001), Sources of organic and inorganic carbon in a headwater stream: Evidence from carbon isotope studies, *Biogeochemistry*, *52*(3), 321–338, doi:10.1023/A%253A1006447706565.

Peter, H., et al. (2014), Scales and drivers of temporal pCO_2 dynamics in an Alpine stream, *J. Geophys. Res. Biogeosci.*, *119*, 1078–1091, doi:10.1002/2013JG002552.

Prairie, Y., and P. del Giorgio (2013), A new pathway of freshwater methane emissions and the putative importance of microbubbles, *Inland Waters*, *3*(3), 311–320.

R Development Core Team (2015), R: A language and environment for statistical computing, in *R Foundation for Statistical Computing*, Vienna, Austria.

Raymond, P. A., J. E. Bauer, and J. J. Cole (2000), Atmospheric CO_2 evasion, dissolved inorganic carbon production, and net heterotrophy in the York River estuary, *Limnol. Oceanogr.*, *45*(8), 1707–1717, doi:10.4319/lo.2000.45.8.1707.

Raymond, P. A., C. J. Zappa, D. Butman, T. L. Bott, J. Potter, P. Mulholland, A. E. Laursen, W. H. McDowell, and D. Newbold (2012), Scaling the gas transfer velocity and hydraulic geometry in streams and small rivers, *Limnol. Oceanogr.: Fluids Environ.*, *2*, 41–53, doi:10.1215/21573689-1597669.

Raymond, P. A., et al. (2013), Global carbon dioxide emissions from inland waters, *Nature*, *503*(7476), 355–359, doi:10.1038/nature12760.

Raymond, P. A., J. E. Saiers, and W. V. Sobczak (2016), Hydrological and biogeochemical controls on watershed dissolved organic matter transport: Pulse-shunt concept, *Ecology*, *97*, 5–16, doi:10.1890/14-1684.1.

Regnier, P., et al. (2013), Anthropogenic perturbation of the carbon fluxes from land to ocean, *Nat. Geosci.*, *6*(8), 597–607, doi:10.1038/ngeo1830.

Revelle, W. (2016), *Psych: Procedures for Personality and Psychological Research*, *Version= 1.5. 8*, Northwestern Univ., Evanston, Ill.

Richey, J. E., et al. (2002), Outgassing from Amazonian rivers and wetlands as a large tropical source of atmospheric CO2, *Nature*, *416*(6881), 617–620, doi:10.1038/416617a.

Richey, J. E. (2004), Pathways of Atmospheric CO_2 through Fluvial Systems, in *Scope-Scientific Committee on Problems of the Environment International Council of Scientific Unions*, vol. 62, pp. 329–340, Island Press, Wash.

Sams, J. I., et al. (2014), Application of near-surface geophysics as part of a hydrologic study of a subsurface drip irrigation system along the Powder River floodplain near Arvada, Wyoming, *Int. J. Coal Geol.*, *126*, 128–139.

Samson, F. B., F. L. Knopf, and W. R. Ostlie (2004), Great Plains ecosystems: Past, present, and future, *Wildl. Soc. Bull.*, *32*(1), 6–15.

Sand-Jensen, K., and P. A. Staehr (2012), CO_2 dynamics along Danish lowland streams: Water–air gradients, piston velocities and evasion rates, *Biogeochemistry*, *111*(1–3), 615–628.

Sanders, I. A., C. M. Heppell, J. A. Cotton, G. Wharton, A. G. Hildrew, E. J. Flowers, and M. Trimmer (2007), Emission of methane from chalk streams has potential implications for agricultural practices, *Freshw. Biol.*, *52*(6), 1176–1186, doi:10.1111/j.1365-2427.2007.01745.x.

Sawakuchi, H. O., D. Bastviken, A. O. Sawakuchi, A. V. Krusche, M. V. R. Ballester, and J. E. Richey (2014), Methane emissions from Amazonian rivers and their contribution to the global methane budget, *Global Change Biol.*, *20*(9), 2829–2840.

Sawakuchi, H. O., et al. (2017), Carbon dioxide emissions along the lower Amazon River, *Front. Mar. Sci.*, *4*, 76.

Schade, J. D., J. Bailio, and W. H. McDowell (2016), Greenhouse gas flux from headwater streams in New Hampshire, USA: Patterns and drivers, *Limnol. Oceanogr.*, *61*, S165–S174, doi:10.1002/lno.10337.

Schelker, J., G. A. Singer, A. J. Ulseth, S. Hengsberger, and T. J. Battin (2016), CO_2 evasion from a steep, high gradient stream network: Importance of seasonal and diurnal variation in aquatic pCO_2 and gas transfer, *Limnol. Oceanogr.*, *61*(5), 1826–1838, doi:10.1002/lno.10339.

Service (2009), *National Wetlands Inventory*, U.S. Fish and Wildlife Service, Dep. of the Interior, Madison, Wisconsin.

Simley, J. D., W. J. Carswell Jr. (2009), USGS fact sheet 2009-3054: The National Map-Hydrography, USGS Fact Sheet, p. 4. [Available at http://pubs.usgs.gov/fs/2009/3054/.]

Smith, L. K., and W. M. Lewis (1992), Seasonality of methane emissions from five lakes and associated wetlands of the Colorado Rockies, *Global Biogeochem. Cycles*, *6*, 323–338, doi:10.1029/92GB02016.

Stackpoole, S. M., E. G. Stets, and R. G. Striegl (2014), The impact of climate and reservoirs on longitudinal riverine carbon fluxes from two major watersheds in the Central and Intermontane West, *J. Geophys. Res. Biogeosci.*, *119*, 848–863, doi:10.1002/2013JG002496.

Stanley, E. H., et al. (2015), The ecology of methane in streams and rivers: Patterns, controls, and global significance, *Ecol. Monogr.*, *86*, 146–171, doi:10.1890/15-1027.1.

Stearns, M., J. A. Tindall, G. Cronin, M. J. Friedel, and E. Bergquist (2005), Effects of coal-bed methane discharge waters on the vegetation and soil ecosystem in Powder River Basin, Wyoming, *Water, Air, Soil Pollut.*, *168*(1–4), 33–57.

Stets, E. G., D. Butman, C. P. McDonald, S. M. Stackpoole, M. D. DeGrandpre, and R. G. Striegl (2017), Carbonate buffering and metabolic controls on carbon dioxide in rivers, *Global Biogeochem. Cycles*, *31*, 663–677, doi:10.1002/2016GB005578.

Striegl, R. G., M. M. Dornblaser, C. P. McDonald, J. R. Rover, and E. G. Stets (2012), Carbon dioxide and methane emissions from the Yukon River system, *Global Biogeochem. Cycles*, *26*, GB0E05, doi:10.1029/2012GB004306.

Survey (2014), *Wyoming Bedrock Geology*, Wyoming State Geol. Surv., Laramie, Wyo. [Available at http://explorer.geospatialhub.org/geo-portal/catalog/search/resource/details.page?uuid=%7BFBD1E59C-88A6-4FCF-951A-E8CFDC4FD481%7D.]

Swenson, H. A. (1953), Geochemical relationships of water in the Powder River basin, Wyoming and Montana, *EOS Trans. Am. Geophys. Union*, *34*(3), 443–448.

Tamooh, F., F. J. R. Meysman, A. V. Borges, T. R. Marwick, K. Van Den Meersche, F. Dehairs, R. Merckx, and S. Bouillon (2014), Sediment and carbon fluxes along a longitudinal gradient in the lower Tana River (Kenya), *J. Geophys. Res. Biogeo.*, *119*, 1340–1353, doi:10.1002/2013JG002358.

Taylor, R. T., D. E. Naugle, and L. S. Mills (2012), Viability analysis for the conservation of sagegrouse populations: Buffalo Field Office, Final Report, 27, Wyoming.

Tilman, D., K. G. Cassman, P. A. Matson, R. Naylor, and S. Polasky (2002), Agricultural sustainability and intensive production practices, *Nature*, *418*(6898), 671–677, doi:10.1038/nature01014.

Tukey, J. W. (1949), Comparing individual means in the analysis of variance, *Biometrics*, 99–114.

Walker, J. C. G., P. B. Hays, and J. F. Kasting (1981), A negative feedback mechanism for the long-term stabilization of Earth's surface temperature, *J. Geophys. Res.*, *86*, 9776–9782, doi:10.1029/JC086iC10p09776.

Wallin, M., I. Buffam, M. Öquist, H. Laudon, and K. Bishop (2010), Temporal and spatial variability of dissolved inorganic carbon in a boreal stream network: Concentrations and downstream fluxes, *J. Geophys. Res.*, *115*, G02014, doi:10.1029/2009JG001100.

Wallin, M. B., M. G. Öquist, I. Buffam, M. F. Billett, J. Nisell, and K. H. Bishop (2011), Spatiotemporal variability of the gas transfer coefficient (KCO_2) in boreal streams: Implications for large scale estimates of CO_2 evasion, *Global Biogeochem. Cycles*, *25*, GB3025, doi:10.1029/2010GB003975.

Wallin, M. B., T. Grabs, I. Buffam, H. Laudon, A. Ågren, M. G. Öquist, and K. Bishop (2013), Evasion of CO_2 from streams–The dominant component of the carbon export through the aquatic conduit in a boreal landscape, *Global Change Biol.*, *19*, 785–797, doi:10.1111/gcb.12083.

Weaver, T. (1980), Climates of vegetation types of the northern Rocky Mountains and adjacent plains, *Am. Midl. Nat.*, *103*, 392–398.

Wetzel, R. G. (2001), *Limnology: Lake and River Ecosystems*, Academic Press, San Diego, Calif.

Wickland, K. P., R. G. Striegl, S. K. Schmidt, and M. A. Mast (1999), Methane flux in subalpine wetland and unsaturated soils in the southern Rocky Mountains, *Global Biogeochem. Cycles*, *13*, 101–113, doi:10.1029/1998GB900003.

Wit, F., D. Müller, A. Baum, T. Warneke, W. S. Pranowo, M. Müller, and T. Rixen (2015), The impact of disturbed peatlands on river outgassing in Southeast Asia, *Nat. Commun.*, *6*, 10155.

Wolock, D. M., and G. J. McCabe (1999), Estimates of runoff using water-balance and atmospheric general circulation models, *J. Am. Water Resour. Assoc.*, *35*(6), 1341–1350, doi:10.1111/j.1752-1688.1999.tb04219.x.

Xian, G., C. Homer, J. Dewitz, J. Fry, N. Hossain, and J. Wickham (2011), Change of impervious surface area between 2001 and 2006 in the conterminous United States, *Photogramm. Eng. Remote. Sens.*, *77*(8), 758–762.